Modeling of Phase Separation in PEG–Salt Aqueous Two-Phase Systems

Paresh U. Kenkare and Carol K. Hall
Dept. of Chemical Engineering, North Carolina State University, Raleigh, NC 27695

A molecular model based on the integral equation theory of statistical thermodynamics is used to study phase separation in PEG–salt aqueous two-phase systems. PEG molecules are modeled as hard spheres that attract each other through a temperature-dependent Yukawa potential, which mimics the effect of PEG–water hydrogen bonding on the attraction between PEG molecules. The salt ions are modeled as charged hard spheres interacting through a Coulombic potential. Excess thermodynamic properties due to Coulombic and Yukawa interactions are calculated by analytical solutions to the Ornstein–Zernike equation for the mean spherical approximation closure. Yukawa parameters for PEG–PEG interactions are determined by fitting the theoretical phase diagram for a pure Yukawa fluid to the experimental phase diagram for a PEG–water mixture. The model predicts experimentally observed trends: increasing the temperature increases the slope and length of the tie lines; increasing the PEG molecular weight increases the miscibility gap; and increasing the anion charge lowers the salt concentration at which phase separation occurs. Theoretical results allow us to infer the relative importance of ion–PEG interactions, ion–solvent interactions, and the interpenetrable nature of PEG molecules on the phase separation in PEG–salt aqueous two-phase systems.

Introduction

Aqueous two-phase systems are formed when two polymers, such as poly(ethylene glycol) (PEG) and dextran, or a polymer and salt, such as PEG and ammonium sulfate, are mixed above their critical concentrations in an aqueous medium (Albertsson, 1986). When biomaterials, such as proteins, are added to these mixtures they partition unequally between the two phases formed. Thus, aqueous two-phase extraction, a technique based on the partitioning of proteins in aqueous two-phase systems, has the potential of being used for the isolation and concentration of biomaterials (Walter et al., 1985; Fisher and Sutherland, 1989). Although aqueous two-phase extraction shows promise for the downstream processing of biomaterials, its use has been hampered by the lack of a comprehensive theory based on fundamental principles that is capable of explaining and predicting the experimental trends observed (Walsh and Headon, 1994). Most of the models developed to describe phase separation and partitioning in aqueous two-phase systems are based on experimental data and are empirical in nature, thus requiring measurement or fitting of a large number of parameters. In order to develop simple models that are capable of explaining and predicting the trends observed in aqueous two-phase systems, it is essential to understand the interactions taking place between the molecular constituents—polymer, salt, proteins, and water—of an aqueous two-phase mixture.

In this article we use a molecular model based in the integral equation theory of statistical thermodynamics to study phase separation in PEG–salt–water systems. We model the phase separation seen in these systems by studying phase separation in a model mixture containing three species—positively and negatively charged hard spheres to mimic the salt ions, and hard spheres with an attraction to mimic the PEG molecules. The potential of interaction between the salt ions is Coulombic, whereas the attraction between the PEG molecules is modeled using an attractive potential of the Yukawa form with well depth ϵ and a range z.

We present a brief review of some of the models devel-

Correspondence concerning this article should be addressed to C. K. Hall.
Current address of P. U. Kenkare: Simons Technologies, Inc., One West Court Square, Decatur, GA 30030.

oped to explain phase separation and protein partitioning in aqueous two-phase systems. More detailed reviews of the theoretical and experimental advances made in this area have been written by Walter and coworkers (1986, 1991), Baskir et al. (1989a), and Abbott et al. (1990). Early modeling work on aqueous two-phase systems was done using the Flory–Huggins theory of polymer solutions. Brooks and coworkers (1985) used the Flory–Huggins theory to develop a lattice model that gives a qualitative description of the phase separation observed in a mixture of polymer solutes. Kang and Sandler (1987, 1988a) combined the Flory–Huggins theory and the UNIQUAC model of Abrams and Prausnitz (1975) to develop models of PEG–dextran aqueous two-phase systems that take into account the effects of polydispersivity (Kang and Sandler, 1988b) and temperature (Hartounian et al., 1993). Diamond and Hsu (1989, 1990) modified the Flory–Huggins theory for polymer solutions to obtain a semiempirical expression for protein partitioning in PEG–dextran aqueous two-phase systems both in the presence and absence of salts. One of the drawbacks of using the Flory–Huggins lattice model is that it treats the protein, which has a compact globular structure, in an unrealistic manner by assuming that it has a loose chainline structure similar to polymers. Baskir et al. (1987) assumed such a globular form for proteins and used the Scheutjens and Fleer's (1979, 1980) lattice theory to develop a model to predict protein partition coefficients in a PEG–PVME [poly(vinyl methyl ether)] aqueous two-phase system (Baskir et al., 1989b).

Virial expansion models provide another approach to studying protein partitioning and phase separation in aqueous two-phase systems. King et al. (1988) and Haynes et al. (1989a,b, 1993) proposed thermodynamic models based on the osmotic virial equation of Ogston (1962) and Edmond and Ogston (1968, 1970) to evaluate protein partition coefficients, phase diagrams, and electrostatic potentials between phases for polymer–polymer and polymer–salt aqueous two-phase systems. The osmotic virial coefficients are obtained from low-angle laser-light scattering data for the aqueous mixtures. The main drawback of these models is that they require the independent determination of several parameters in order to calculate the free energy of the system. Forciniti and Hall (1990) and Cabezas et al. (1989, 1990) have developed models for aqueous two-phase extraction using a virial expansion approach based on the constant pressure solution theory of Hill (1960). The work of Forciniti and Hall (1990) suggests that excluded volume forces alone are not sufficient to explain trends obtained for protein partitioning in aqueous two-phase systems. Guan and coworkers (1993a) have, however, questioned the application of virial expansion models to study aqueous two-phase systems by showing that a thermodynamic inconsistency is present in the virial expansions that precludes their use in phase equilibria calculations. Recently, Döbert and coworkers (1995) have derived thermodynamically consistent expressions for the Gibbs free energy and the chemical potential of the solute based on the osmotic virial equation. However, the osmotic virial coefficients have to be calculated from experimental data on water activities in solutions of PEG and dextran of varying molecular weight.

An alternative approach to modeling phase separation in PEG–dextran and PEG–salt aqueous two-phase systems has been provided by Guan et al. (1993b, 1994). They obtain binodal curves for aqueous two-phase systems by assuming that the PEG and dextran (or PEG and salt) molecules are distributed in the solution according to a probability given by the molecules' effective excluded volume. However, in order to account for attractive interactions in the solution, they too have to extend their model to include experimentally determined parameters for the second virial expansion of the solvent (Guan et al., 1993a).

Many of the models developed for aqueous two-phase systems involve the evaluation of several parameters, such as second virial coefficients, from experimental data. Although the use of additional parameters improves the quantitative predictions of the model, it also makes it difficult to gauge the relative importance of the contributions represented by these parameters on model predictions. In this work we adopt a simple three-parameter molecular model to study PEG–salt aqueous two-phase systems. This simple model demonstrates the role that salts play in reducing the temperature at which PEG–salt–water mixtures phase separate. The PEG molecules are modeled as neutral hard spheres interacting with each other through a temperature-dependent attractive Yukawa potential and the salt ions are modeled as charged hard spheres interacting via a Coulombic potential. Three adjustable parameters determine the form of the PEG–PEG Yukawa attraction and are used to fit the salt-free theoretical PEG–water phase diagram to the salt-free experimental PEG–water phase diagram. Once these parameters are determined for each PEG molecular weight, the phase diagrams for the PEG–water mixtures in the presence of salts are evaluated without the use of any additional adjustable parameters. In our work we also study the role that Coulombic interactions play on phase separation in PEG–salt–water systems at very low temperatures. It has been well established that the presence of Coulombic interactions alone can cause phase separation (Coulombic phase separation). This work theoretically evaluates and discusses the possibility of Coulombic phase separation at low temperatures in aqueous two-phase systems containing salts.

Analytical expressions for the thermodynamic properties of models with pure hard sphere, Coulombic, or Yukawa interactions have been previously obtained by other investigators. We combine these expressions to obtain the total thermodynamic properties of our model mixture since it contains all three types of interactions. The excess (over an ideal gas) thermodynamic properties due to hard sphere interactions are taken from the Mansoori–Carnahan–Starling–Leland (1971) equation of state for hard-sphere mixtures. The excess thermodynamic properties (over a hard-sphere system) due to Coulombic interactions are taken from Blum (1975) and Blum and Hoye's (1977) MSA solution algorithm for charged hard-sphere mixtures. The MSA, when applied to hard spheres interacting via the coulombic potential, extends the classic Debye–Hückel theory for ionic solutions so as to account for finite ion size. Finally, the excess thermodynamic properties (over a hard-sphere system) due to the Yukawa attractions are taken from Arrieta et al.'s (1987) MSA solution algorithm for a pure Yukawa fluid. The numerical procedure used for phase-diagram calculation has been adopted from an algorithm developed by Kenkare and coworkers (1995a,b, 1996) to study phase separation in charged hard-sphere mixtures.

We have obtained phase diagrams in the temperature vs.

PEG weight fraction, temperature vs. salt weight fraction, and PEG vs. salt weight fraction (binodal curve) planes for model PEG–salt–water mixtures. The model predicts that the addition of salts to a PEG–water mixture decreases the lower critical solution temperature (LCST) of the mixture. We also model the effect of temperature, PEG molecular weight, and salt type on the theoretical PEG–salt binodal curves and compare with the trends seen in experiment. The model correctly predicts that increasing the temperature and increasing the molecular weight of the PEG increases the miscibility gap in the PEG–salt binodal curve. Also, as is experimentally observed, an increase in anion charge moves the binodal curves toward lower salt concentrations. The model phase diagrams, however, underestimate the equilibrium salt concentrations and predict a higher LCST than that observed experimentally. The model also cannot convincingly distinguish between the binodal curves of salts that have the same charges on them [e.g., Na_2SO_4, $(NH_4)_2SO_4$, and Li_2SO_4]. These discrepancies probably indicate that ion–solvent effects such as hydration and PEG–salt interactions, both of which are ignored in our model, play an important role in PEG–salt aqueous two-phase separation.

The remainder of this article is organized as follows. The next section describes the interaction potentials used in our model, and the following section explains the Ornstein–Zernike equation and the MSA closure used to solve it. We then present a derivation of the thermodynamic expressions for the osmotic pressure and the Gibbs free energy of the model mixture and also briefly describe the numerical technique used for phase-diagram calculation. In the Result section we obtain PEG–water and PEG–salt–water phase diagrams for a variety of salts at a range of temperatures and PEG molecular weights and compare with the trends seen in experiments. Finally, we conclude with a summary of the theory's predictions.

Potentials of Interaction

In our model mixture, species 1 and 2, which represent the salt cation and anion, respectively, contain particles of diameter d_1 and d_2 and charge $z_1 > 0$ and $z_2 < 0$, and species 3, which represents the PEG molecules, contains neutral particles of diameter d_3. The water is represented by a structureless continuum of dielectric constant, $\epsilon_d = 78.4$. Thus the interaction potential between the different solute species (PEG and salt ions) is a solvent-averaged potential of mean force, and the mixture is treated within the framework of the McMillan–Mayer theory.

The potential of interaction, $u_{ij}(r)$, between the ions ($i = 1, 2$; $j = 1, 2$) is Coulombic and is given by the expression,

$$u_{ij}(r) = \infty \qquad r \le d_{ij}$$
$$u_{ij}(r) = \frac{z_i z_j e^2}{\epsilon_d r} \qquad r > d_{ij}, \tag{1}$$

where r is the distance between the centers of ions of types i and j, $d_{ij} = (d_i + d_j)/2$, and $e = 4.8 \times 10^{-10}$ e.s.u is the charge on one electron in CGS units.

We have used a temperature-dependent Yukawa attraction to model the interaction between the PEG molecules in solution. Thermodynamic models for PEG–water phase diagrams show that the intermolecular interactions in the mixture are strongly temperature-dependent. Kjellander and Florin (1981), and Goldstein (1984) have attributed this temperature-dependence to the role that hydrogen-bonding forces play when PEG molecules interact with each other in an aqueous medium. An alternative explanation has been provided by Karlström (1985), who suggests that changes in PEG chain structure with temperature may be responsible for the observed phase diagrams. In either case, an increase in temperature leads to an increase in attraction between the PEG molecules. The attraction between the PEG molecules is modeled by using an attractive Yukawa potential, $u_{33}(r)$, of the form,

$$u_{33}(r) = \infty \qquad r \le d_3$$
$$= -\frac{\epsilon}{(r/d_3)} \exp\left[-z\left(\frac{r}{d_3} - 1\right)\right] \qquad r > d_3, \tag{2}$$

where ϵ is the depth of the attractive well and z is the range of the potential. The increase in PEG–PEG attraction with increasing temperature is modeled by making the well-depth ϵ (in Eq. 2) an increasing function of temperature, T,

$$\epsilon = k_B T/(A - BT), \tag{3}$$

where A and B are constants and k_B is Boltzmann's constant. In our model the constants A, B, and z are fit to make the theoretically predicted temperature–PEG weight fraction binodal curve match the experimentally observed temperature–PEG weight fraction phase diagram for a PEG–water system.

The potential of interaction between the ions (species 1 and 2) and the PEG molecules (species 3) is assumed to be hard-sphere repulsion alone. Since ions are penetrable to the larger PEG molecules, a more realistic potential would probably include an attractive term inside the hard core [$r < (d_i + d_j)/2$]. We, however, neglect ion–PEG dispersion forces because including them would make analytical evaluation of thermodynamic properties difficult, and this in turn would make phase-diagram calculations numerically intractable.

Ornstein–Zernike Equation and the MSA Closure

The thermodynamic properties of our model mixture are evaluated within the framework of the integral-equation theory in statistical thermodynamics. The integral-equation theory is grounded in the Ornstein–Zernike equation, which for a multicomponent system containing l species, is written as (Lee, 1988),

$$h_{ij}(r) = c_{ij}(r) + \sum_l \rho_l \int c_{il}(r) h_{lj}(r) dr \tag{4}$$

where r is the distance between two molecules of species i and species j; ρ_l is the number density of species l; $h_{ij}(r)$ is the total correlation function between molecules of species i and species j and is related to the radial distribution function $g_{ij}(r)$ through the equation $h_{ij}(r) = g_{ij}(r) - 1$; and $c_{ij}(r)$ is

the direct correlation function between two molecules of species i and species j. Physically, Eq. 4 means that the total correlation, $h_{ij}(r)$, between a molecule of species i and a molecule of species j contains two contributions: a direct correlation, $c_{ij}(r)$, and an indirect correlation that is propagated through the other molecules, l, in the mixture. The indirect correlation (given by the second term on the RHS of Eq. 4) is averaged over all positions of the molecules and is weighted by the number density of each of the species in the mixture. The Ornstein–Zernike equation is useful to liquid-state theorists because all thermodynamic properties for the mixture can be evaluated in terms of $h_{ij}(r)$ and $c_{ij}(r)$. In order to solve the Ornstein–Zernike equation for $h_{ij}(r)$ and $c_{ij}(r)$, it is necessary to postulate a second relationship between these two functions called the closure that is based on physically reasonable arguments. Insertion of the closure into the Ornstein–Zernike relation leads to a closed-integral equation for $h_{ij}(r)$ that can be solved either analytically or numerically.

In this article we use the mean spherical approximation (MSA) closure for the Ornstein–Zernike equation to evaluate excess thermodynamic properties associated with the Coulombic and Yukawa interactions in our mixture. The MSA closure (Hansen and McDonald, 1991) is defined by

$$\begin{aligned} h_{ij}(r) &= -1 \qquad r < d_{ij} = (d_i + d_j)/2 \\ c_{ij}(r) &= -\beta u_{ij} \qquad r > d_{ij}, \end{aligned} \tag{5}$$

where u_{ij} is the pair potential between species i and j, and $\beta = (k_B T)^{-1}$ with k_B equal to Boltzmann's constant. Physically the MSA closure says that (1) inside the hard core ($r < d_{ij}$) the radial distribution function is zero, which is exact; and (2) outside the hard core the direct correlation function is equal to the pair potential between the molecules, an assumption that is exact in the limit of large r. The advantage of using the MSA closure is that it allows for an analytical solution to the Ornstein–Zernike equation for the Coulombic and Yukawa interaction potentials (Eqs. 1 and 2, respectively). Thus, simple analytical expressions (or sets of equations that can be solved numerically) have been developed for the thermodynamic properties of a mixture of hard spheres interacting either by the Coulombic potential (Blum, 1975; Blum and Hoye, 1977) or the Yukawa potential (Arrieta et al., 1987).

Thermodynamic Properties and Phase Equilibria Calculations

In this section we derive expressions for the osmotic pressure and the Gibbs free energy of our model mixture and present the method used for evaluating phase diagrams. Thermodynamic properties of the mixture are calculated by summing up the individual contributions associated with the intermolecular potentials between the various species in our model mixture.

Consider a model mixture of salt $R_{\nu_1}S_{\nu_2}$ and PEG (species 3), where ν_1 and ν_2 are the stoichiometric coefficients of the cation R (species 1) and anion S (species 2), respectively. The mole fraction, c, of the salt ($R_{\nu_1}S_{\nu_2}$) in the model mixture can be written as

$$c = \frac{\rho_1}{\rho_1 + \rho_3 \nu_1} \tag{6}$$

where ρ_i, the number density of species i, is defined as the ratio of the number of particles, N_i, of species i, to the volume, V, of the mixture. By combining Eq. 6 with the electroneutrality condition, $\rho_1\nu_2 - \rho_2\nu_1 = 0$, we can express the species number fraction, $x_i \left(= \rho_i / \sum_{i=1}^{3} \rho_i \right)$ in terms of the salt mole fraction c as

$$\begin{aligned} x_1 &= \frac{c\nu_1}{1 + c(\nu_1 + \nu_2 - 1)} \\ x_2 &= \frac{c\nu_2}{1 + c(\nu_1 + \nu_2 - 1)} \\ x_3 &= \frac{1 + c}{1 + c(\nu_1 + \nu_2 - 1)}. \end{aligned} \tag{7}$$

The total number of particles in the mixture,

$$N_t^{\text{part}} \left(= \sum_{i=1}^{3} N_i \right),$$

is related to the total number of molecules in the mixture, N_t^{mol}, by the expression

$$N_t^{\text{part}} = [1 + c(\nu_1 + \nu_2 - 1)] N_t^{\text{mol}}. \tag{8}$$

The total Gibbs free energy of the mixture can be written as the sum of an ideal contribution, an excess hard-sphere contribution, an excess Coulombic contribution, and an excess contribution due to Yukawa attractions. The ideal and hard-sphere contributions to the reduced Gibbs free energy, g^{id} and g^{hs}, account for the ideal and hard sphere interactions between all the species of the mixture; the Coulombic contribution, g^{coul}, accounts for the Coulombic interactions between the charged species (species 1 and 2); and the Yukawa contribution, g^{yuk}, accounts for the Yukawa attraction between the particles of species 3. Hence, the reduced total Gibbs free energy of the mixture may be written as

$$\begin{aligned} \beta G = N_t^{\text{part}} g^{id}(T,V) + N_t^{\text{part}} g^{hs}(T,V) \\ + (N_1 + N_2) g^{\text{coul}}(T,V) + N_3 g^{\text{yuk}}(T,V) \end{aligned} \tag{9}$$

The ideal contribution to the Gibbs free energy per particle is given by

$$g^{id} = \sum_{i=1}^{3} x_i \ln(\rho_i \Lambda_i^3), \tag{10}$$

where $\Lambda_i = (2\pi m_i k_B T/h^2)^{-1/2}$ is the thermal De Broglie wavelength; h is Planck's constant; and m_i is the mass of species i. The excess hard-sphere Gibbs free energy per particle, $g^{hs}(T, V)$, is excess over an ideal gas at the same temperature and volume and is obtained for the mixture of

species 1, 2 and 3 using Mansoori et al.'s (1971) equation of state. [To obtain an expression for the excess hard-sphere Gibbs free energy over an ideal gas at the same temperature and volume, the ln Z term has to be dropped from the excess hard-sphere Gibbs free energy expression in the reference by Mansoori et al. (1971).] The excess Coulombic Gibbs free energy per particle, $g^{\text{coul}}(T, V)$, is excess over a hard-sphere system at the same temperature and volume and is obtained for a mixture of the charged species 1 and 2 using the analytical solution to the MSA derived by Blum and Hoye (1975, 1977). The excess (over a hard-sphere system) Gibbs free energy per particle due to Yukawa interactions, $g^{\text{yuk}}(T, V)$, is obtained for pure species 3 using Arrieta et al.'s (1987) MSA solution algorithm to the Ornstein–Zernike equation.

The total Gibbs free energy per molecule of the mixture is obtained by substituting N_t^{part} in terms of N_t^{mol} (using Eq. 8), and x_i in terms of c (using Eq. 7), into Eq. 9,

$$\begin{aligned}\beta G/N_t^{\text{mol}} &= c\nu_1 \ln \rho_1\Lambda_1^3 + c\nu_2 \ln \rho_2\Lambda_2^3 + (1-c)\ln \rho_3\Lambda_3^3 \\ &+ [1 + c(\nu_1+\nu_2-1)]g^{hs}(T,V) + c(\nu_1+\nu_2)g^{\text{coul}}(T,V) \\ &+ (1-c)g^{\text{yuk}}(T,V). \quad (11)\end{aligned}$$

Since the addition of constants or terms linear in mole fraction to the Gibbs free energy does not affect the phase-diagram calculations, we subtract these terms from the preceding expression, to arrive at a simpler expression for the Gibbs free energy per molecule of the mixture, G^*,

$$\begin{aligned}G^* \equiv \beta G/N_t^{\text{mol}} &- c\nu_1 \ln \Lambda_1^3 - c\nu_2 \ln \Lambda_2^3 - (1-c)\ln \Lambda_3^3 \\ &= c\nu_1 \ln \rho_1 + c\nu_2 \ln \rho_2 + (1-c)\ln \rho_3 \\ &+ [1 + c(\nu_1+\nu_2-1)]g^{hs}(T,V) \\ &+ c(\nu_1+\nu_2)g^{\text{coul}}(T,V) + (1-c)g^{\text{yuk}}(T,V). \quad (12)\end{aligned}$$

The analytical expressions for $g^{hs}(T, V)$ and $g^{\text{coul}}(T, V)$ are given in the appendix of an earlier article by Kenkare et al. (1995a).

The osmotic pressure of the mixture, P, is evaluated from the total compressibility factor, Z, of the mixture using the relationship $Z = \beta P/\rho$, where $\rho\left(=\sum_{i=1}^{3}\rho_i\right)$ is the total density of the mixture. The total compressibility factor, Z, is the sum of the hard-sphere contributions to the osmotic pressure, Z^{hs} (which includes the ideal contribution), the excess Coulombic contribution to the compressibility factor (over a hard-sphere system), Z^{coul}, and the excess Yukawa contribution to the compressibility factor (over a hard-sphere system), Z^{yuk}. The total osmotic pressure of the mixture is given by the expression

$$P = [Z^{hs} + (x_1+x_2)Z^{\text{coul}} + x_3 Z^{\text{yuk}}]\rho k_B T, \quad (13)$$

where Z^{hs} is evaluated for the mixture of species 1, 2 and 3, using Mansoori et al.'s (1971) equation of state; Z^{coul} is obtained for the mixture of charged species 1 and 2 using the analytical solution to the MSA derived by Blum and Hoye (1975, 1977); and Z^{yuk} is obtained for pure species 3 using Arrieta et al.'s (1987) MSA solution algorithm. The analytical expressions for Z^{hs} and Z^{coul} (also known as the osmotic coefficient, ϕ^{coul}) are given in the appendix of an earlier article by Kenkare et al. (1995a).

Phase equilibrium for our model mixture is evaluated by determining the mole fractions, c^α and c^β, of the phases α and β, respectively, at which the temperature, T, osmotic pressure, P, and chemical potential, μ_i, of each compound is the same in both phases. Mathematically this may be written as

$$\begin{aligned}\mu^\alpha_{\text{salt}}(T,P,c^\alpha) &= \mu^\beta_{\text{salt}}(T,P,c^\beta) \\ \mu^\alpha_{\text{PEG}}(T,P,c^\alpha) &= \mu^\beta_{\text{PEG}}(T,P,c^\beta), \quad (14)\end{aligned}$$

where the chemical potentials of the salt and PEG, μ_{salt} and μ_{PEG}, respectively, can be calculated as a function of mole fraction, c, from the total Gibbs free energy, G^*,

$$\begin{aligned}\mu_{\text{salt}} &= G^* + (1-c)\left(\frac{\partial G^*}{\partial c}\right)_{T,P} \\ \mu_{\text{PEG}} &= G^* - c\left(\frac{\partial G^*}{\partial c}\right)_{T,P}. \quad (15)\end{aligned}$$

The Gibbs free energy, G^*, is obtained as a function of c at constant T and P using a numerical procedure described in an earlier article by Kenkare et al. (1995a). The chemical potentials of the salt and PEG are then calculated using Eq. 15, and the equilibrium mole fractions c^α and c^β at which the conditions in Eq. 14 are satisfied are determined. By evaluating the equilibrium mole fractions and volume fractions at either fixed osmotic pressure or fixed temperature, we can obtain constant-pressure $T-c$ and $T-\eta$ coexistence curves or constant-temperature $P-c$ and $P-\eta$ coexistence curves, respectively.

Results and Discussion

In this section we use the procedure described earlier to evaluate phase diagrams for our model PEG–water mixtures both in the presence and absence of salts. We limit our modeling efforts to mixtures containing PEG of molecular weights less than 10,000—namely PEG 2180, PEG 5000, and PEG 8000—because our assumption of a globular geometry for PEG molecules in solution, which allows us to model them as hard spheres, is unrealistic for higher molecular weights. Abbott and coworkers (1991, 1992a,b,c, 1993) find that the structure of the PEG solution changes from globular-like to network-like as the PEG molecular weight increases. They determined that at molecular weights greater than 10,000 the PEG molecules lose their globular nature and exist as a network in the solution (Abbott et al., 1991).

The PEG–water system is modeled as a pure fluid containing PEG molecules that interact via a temperature-dependent Yukawa potential of the form given by Eqs. 2 and 3. The values for the Yukawa parameters, z, A, and B are determined at each PEG molecular weight such that the theoretical temperature–PEG weight-fraction phase diagram agrees with the experimental temperature–PEG weight-fraction phase diagrams.

The PEG–salt aqueous two-phase system is modeled as a binary mixture of a Yukawa fluid, representing the PEG molecules, and positively and negatively charged hard spheres, representing the salt. The theoretical temperature–PEG weight-fraction and temperature-salt weight-fraction phase diagrams are determined for the mixture and compared to the corresponding experimental diagrams. Theoretical PEG–salt binodal curves are obtained for the system and compared to experimentally determined PEG–salt binodal curves. The effect of PEG molecular weight, temperature, and salt type on the PEG–salt binodal curve is studied and the observed trends are compared to experiments.

Modeling of PEG–water phase separation: Determining z, A, and B

We now determine values for the Yukawa potential parameters, z, A, and B, that make the theoretical PEG–water phase diagrams for PEG of molecular weights 2,180, 5,000, and 8,000 agree with the experimental PEG–water phase diagrams measured by Saeki et al. (1976) and Malcolm and Rowlinson (1957). The experimental PEG–water phase diagram is generally plotted in the $T-w$ plane, where w is the PEG weight fraction, whereas the theoretical phase diagram of a pure Yukawa fluid is most naturally plotted in the $T^*-\eta$ plane, where $T^*(\equiv k_BT/\epsilon)$ is the reduced temperature and $\eta=\pi\rho d^3/6$ is the volume fraction of the PEG, with ρ and $d(=d_3)$ equal to the number density and diameter of the PEG molecules, respectively. In order to compare the experimental PEG–water phase diagram and the theoretical phase diagram for the Yukawa fluid, we have to convert the theoretical $T^*-\eta$ phase diagram into a theoretical T^*-w phase diagram. The PEG weight fraction, w, can be determined from the PEG volume fraction, η, through the correlation,

$$w=\eta/\{n+(1-\eta)[\,\rho_{\text{water}}N_{Av}\pi d_3^3/(6M)]\}, \qquad (16)$$

where $\rho_{\text{water}}(=1\ \text{g/cm}^3)$ is the density of water; $N_{Av}(=6.023\times10^{23})$ is Avogadro's number; and M is the molecular weight of the PEG. Hence if the diameter, d_3, of the PEG molecules of molecular weight M is determined, the theoretical $T^*-\eta$ phase diagram can be converted into a theoretical T^*-w phase diagram by using the preceding correlation.

The diameter of the PEG molecules is obtained by determining the hydrodynamic volume, $V_h(=\pi d_3^3/6)$, of the molecules. The hydrodynamic volume, V_h, is related to the intrinsic viscosity, $[\eta]$, and the molecular weight, M, of the polymer through the equation (Young and Lovell, 1991);

$$V_h=\frac{2}{5}[\eta]M/N_{Av}, \qquad (17)$$

where $[\eta]$, for a PEG solution of molecular weight $200<M<8{,}000$, is related to M through the equation (Young and Lovell, 1991; Atha and Ingham, 1981),

$$[\eta]=0.156M^{0.5}. \qquad (18)$$

Table 1 contains the diameter of PEG molecules as a function of molecular weight calculated using Eqs. 17 and 18. Using the preceding equations to calculate the size of the PEG molecules gives us the flexibility to extend our model to various other PEG molecular weights (in the range 200 to 8,000) with ease.

Table 1. Data on the Diameter, d_3,* the Critical Experimental Weight Fraction, w_c, the Critical Volume Fraction, η_c,† the Yukawa Range Parameter, z,†† and the Yukawa Well-Depth Parameters A and B, for PEG Species of Different Molecular Weights**

Species	d_3 Å	w_c	η_c	z	A	B (K^{-1})
PEG 2180	27.2	0.24	0.48	22.8	0.42	4.19×10^{-4}
PEG 5000	41.2	0.17	0.47	22.2	1.20	2.44×10^{-3}
PEG 8000	52.1	0.07	0.28	6.5	3.83	8.75×10^{-3}

*Obtained using Eqs. 18 and 17.
**Obtained from the work of Saeki et al. (1976) and Malcolm and Rowlinson (1957).
†Evaluated using Eq. 16.
††Evaluated from η_c using Eq. 19.

In our model the value assigned to the range parameter, z, determines the critical volume fraction, η_c, and hence the critical weight fraction, w_c, that will characterize the theoretical PEG–water phase diagram. We have obtained a correlation between z and the theoretically predicted value of η_c by evaluating $T^*-\eta$ phase diagrams for a pure Yukawa fluid at several values of z (see Figure 1). The critical volume fraction of the pure Yukawa fluid is related to the range parameter z through the approximate correlation

$$z=-7.74+83.91\eta_c-223.2\,\eta_c^2+377.9\eta_c^3 \qquad (0.1<\eta_c<0.5). \qquad (19)$$

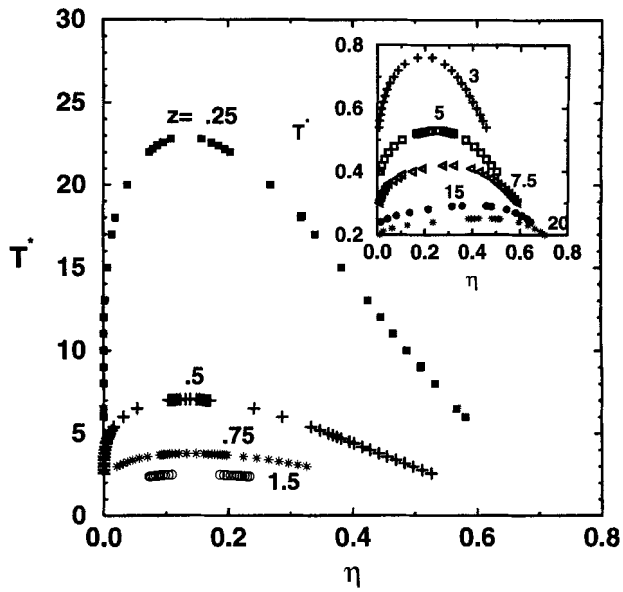

Figure 1. Coexistence in the reduced temperature (T^*)–volume fraction (η) plane for a pure Yukawa fluid at different values of the Yukawa range parameter, z.

The inset magnifies the phase diagrams seen at low temperatures for high values of z. The correlation between the critical volume fraction, η_c, and z given by Eq. 19 is obtained by determining the value of η_c for each value of z from the above graph.

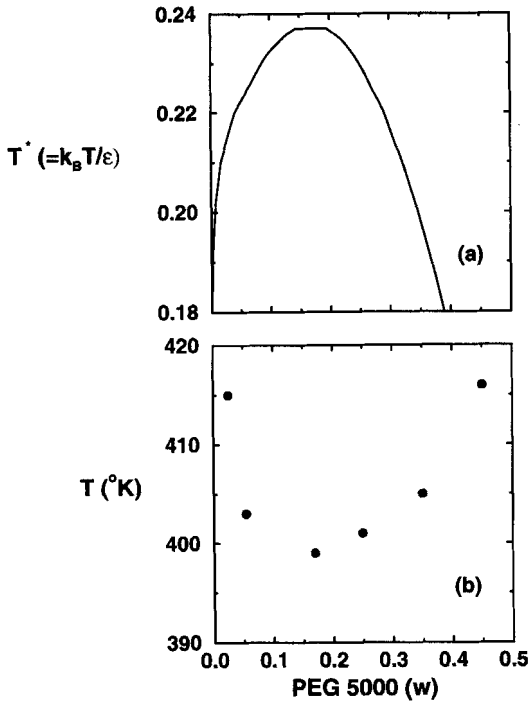

Figure 2. (a) Coexistence in the reduced temperature (T^*)–weight fraction (w) plane for a pure Yukawa fluid with an attractive well-depth, ϵ, and range, $z = 22.2$; (b) experimental phase diagram in the temperature–weight fraction plane for a PEG 5000–water mixture.

The experimental data points (filled circles) are obtained from the work of Malcolm and Rowlinson (1957).

The z value for our PEG–water model mixture is chosen such that the theoretical critical weight fraction fits the experimentally determined critical weight fraction for the PEG–water system. For a given experimental w_c value [obtained from the experimental data of Saeki et al. (1976) and Malcolm and Rowlinson (1957)], the corresponding η_c is evaluated using Eq. 16. The Yukawa range parameter z is then obtained by using the correlation given by Eq. 19. Table 1 presents values for w_c, η_c, and z for the PEG species considered in this article.

The values for z and d_3 determined earlier are used to obtain a theoretical temperature–volume fraction ($T^* - \eta$) phase diagram for the PEG–water system. This phase diagram is converted into a theoretical temperature–weight fraction ($T^* - w$) phase diagram by relating η to w using Eq. 16. Figure 2a shows the phase diagram in the $T^* - w$ plane of a pure Yukawa fluid that mimics the experimental PEG 5000–water system. The Yukawa fluid contains hard spheres, representing the PEG molecules of size $d = 41.2$ Å, interacting by a Yukawa potential of well depth ϵ and range $z = 22.2$. Figure 2b plots the experimental phase diagram for a PEG 5000–water system based on the work of Malcolm and Rowlinson (1957). The phase diagram in Figure 2a ends in an upper critical solution temperature (since the reduced well-depth ϵ/k_BT has no functional dependence on T), whereas the experimental phase diagram in Figure 2b ends in a LCST. The theoretical phase diagram can be converted into a curve ending in a LCST by introducing a temperature dependence into ϵ of the form shown in Eq. 3.

We choose values for A and B (which fix the temperature dependence of the well depth ϵ) to make the theoretical phase diagram in Figure 2a agree with the experimental phase diagram in Figure 2b. At each data point (value of w) appearing in Figure 2b, we determine the associated value of T from Figure 2b and the value of $T^* \equiv k_BT/\epsilon$ from Figure 2a. In Figure 3 we plot the resulting relationship (filled circles) between $\epsilon/k_B (= T/T^*)$ and T for each of the data points in Figure 2b and choose values for A and B such that the functional dependence of ϵ/k_b on T passes through these points. The solid line in Figure 3 shows that for values of $A = 1.2$ and $B = 2.44 \times 10^{-3}$ the ϵ/k_B vs. T plot (solid line) passes through the data points (filled circles). From Figure 3 it might at first seem that a linear line passing through the data points would provide the best fit. However, a linear plot through the data points would intersect the x-axis at $T = 350$ K, implying that for $T \leq 350$ K the well-depth $\epsilon/k_b = 0$, or that there is no attraction between the PEG molecules. In reality at temperatures below the critical temperature ($T < 399$ K), the attraction between the PEG molecules decreases but does not become zero. We find that the fit of $\epsilon/k_B = T/(A - BT)$, which we have used in Figure 3, incorporates the essential features of phase separation in PEG–water systems. At temperatures above the critical temperature there is a rise in ϵ/k_B, signifying stronger attraction between the PEG molecules, thereby leading to phase separation, and at temperatures below the critical point there is a gradual decrease in ϵ/k_B, signifying weaker attraction between the PEG molecules either due to increased hydrogen bonding between the PEG and water molecules, or due to a change in PEG chain structure at lower temperatures. The method just described was also used to obtain values of A and B for PEG–water solutions containing PEG of molecular weights 2,180 and 8,000 (see Table 1). The function $\epsilon/k_B = T/(A - BT)$ goes to infinity at $T = A/B$ (i.e., at $T = 1{,}002$ K for PEG 2180, 492 K for PEG 5000, and 438 K for PEG 8000). However, this does not affect our calculations because the tem-

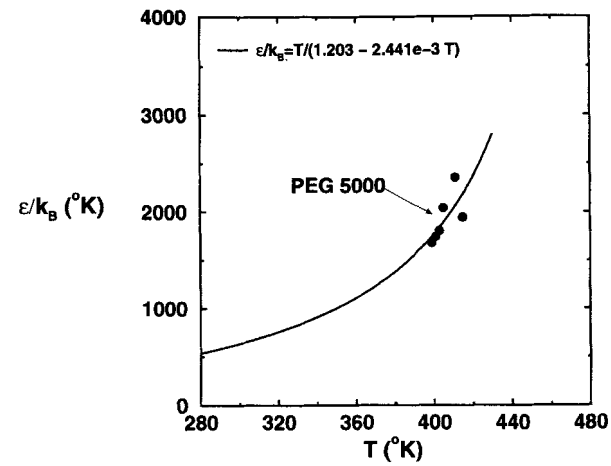

Figure 3. Correspondence between ϵ/k_B and T (or alternatively between T^* and T) (●) for each data point in Figure 2b; functional dependence of well-depth ϵ/k_B on temperature, T(——).

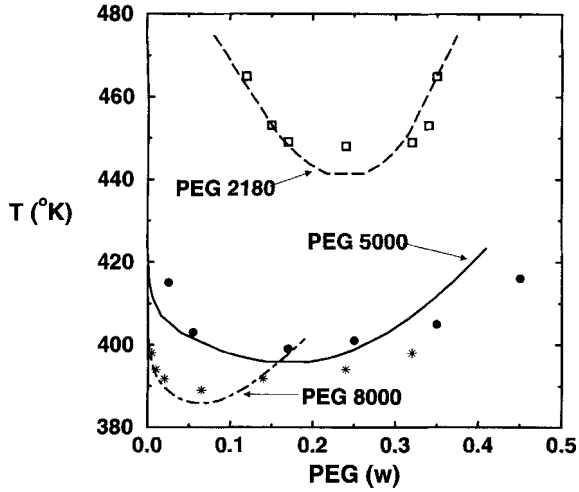

Figure 4. Theoretical and experimental phase diagrams for PEG–water mixtures at different PEG molecular weights.

The lines represent the theoretical coexistence curves and the symbols represent the data points obtained from the experimental phase diagrams of Malcolm and Rowlinson (1957) and Saeki et al. (1976). The theoretical phase diagrams are determined using the values for z, A, and B given in Table 1.

peratures at which ϵ/k_B goes to infinity are significantly higher than the temperatures at which we work.

The values for A and B determined earlier are used to obtain the theoretical $T-w$ phase diagram corresponding to the T^*-w phase diagram shown in Figure 2a. This is done by recognizing that the relationship $\epsilon/k_B = T/(A-BT)$ is equivalent to setting $T^* = A - BT$ and then rescaling the T^*-w phase diagram by determining the T corresponding to each value of T^* in Figure 2a. Figure 4 shows the resulting theoretical $T-w$ phase diagram along with the experimental phase diagram for a PEG–water mixture containing PEG of molecular weights 2,180, 5,000, and 8,000. The experimental data points for PEG 2180 and 8000 were obtained from the phase diagrams of Saeki et al. (1976). A good fit is obtained between the theoretical and experimental phase diagrams for PEG–water mixtures containing PEG 2180 and PEG 5000. The fit in the PEG 8000 curve is not as satisfactory because the theoretical curve is not as broad as the experimental curve. This is probably because our theory overestimates the excluded volume of the PEG molecules by modeling them as hard spheres. At the higher PEG molecular weights, the PEG-rich phase gets saturated at a lower equilibrium PEG concentration than that observed experimentally because the large-sized hard-sphere PEG molecules prevent the other PEG molecules from entering into this phase. In reality, however, the PEG molecules are interpenetrable and can pack themselves effectively, thus resulting in higher equilibrium concentrations of the PEG in the PEG-rich phase.

Phase separation in PEG–salt–water systems

We now obtain phase diagrams for PEG–water mixtures in the presence of salts. The salt ions are modeled as positively and negatively charged hard spheres interacting by the Coulombic potential (Eq. 1). The size of the anions and cations are assumed to be equal to the crystalline hard-core

Table 2. Crystalline Cation and Anion Diameters, d_1 and d_2,* Respectively, for the Salts Considered in this Study**

Cation	d_1 Å	Anion	d_2 Å
Li^+	1.2	OH^-	2.8
Na^+	1.9	SO_4^{2-}	4.58
NH_4^+	2.96	PO_4^{3-}	3.12
Zn^{2+}	1.48		
Al^{3+}	1.0		

*Obtained from Monk (1961).
**For SO_4^{2-} the crystalline diameter was not available, and the solvated diameter is used instead.

diameters. We further assume that the presence of salt ions does not affect the Yukawa parameters for the attraction between the PEG molecules. Hence, we use the values for z, A, and B determined in the previous section (see Table 1).

Evaluation of PEG 2180–$(NH_4)_2SO_4$–Water Phase Diagrams. In this section we obtain temperature–PEG weight fraction and temperature–$(NH_4)_2SO_4$ weight-fraction phase diagrams for a model PEG 2180–$(NH_4)_2SO_4$–water mixture. The trends exhibited by our model are compared to the experimental results of Voros and coworkers (1993), who measured liquid–liquid phase equilibria for a PEG 2000–$(NH_4)_2SO_4$–water mixture at four different temperatures.

The model calculations are performed by setting the diameters of the salt ions equal to the crystalline hard-core diameanion diameters for all the salts considered in this study (for SO_4^{2-} the crystalline diameter data are not available and the solvated diameter is used instead). The weight fraction of the PEG and salt [$(NH_4)_2SO_4$] in each phase are calculated using the expressions,

$$\text{PEG w/w} \equiv \frac{M_3\rho_3}{M_1\rho_1 + M_2\rho_2 + M_3\rho_3 + N_{Av}(1-\eta)}, \quad (20)$$

$$\text{salt w/w} \equiv \frac{M_1\rho_1 + M_2\rho_2}{M_1\rho_1 + M_2\rho_2 + M_3\rho_3 + N_{Av}(1-\eta)}, \quad (21)$$

where M_i and ρ_i are the atomic weights (molecular weight for $i=3$) and number densities, respectively, of species i in the phase, and $\eta(=\sum_{i=1}^{3}\pi\rho_i d_i^3/6)$, is the total volume fraction of the phase. The number densities, ρ_i, of species i in each phase are related to the equilibrium values for the salt mole fraction, c, and the total volume fraction, η, through the expressions,

$$\rho_1 = \frac{6\eta c\nu_1}{\pi[c\nu_1 d_1^3 + c\nu_2 d_2^3 + (1-c)d_3^3]} \quad (22)$$

$$\rho_2 = \rho_1\nu_2/\nu_1 \quad (23)$$

$$\rho_3 = \frac{6\eta(1-c)}{\pi[c\nu_1 d_1^3 + c\nu_2 d_2^3 + (1-c)d_3^3]}. \quad (24)$$

Figures 5a and 5b show our model's predictions for the phase diagram of a PEG 2180–$(NH_4)_2SO_4$–water mixture in the temperature–PEG weight-fraction plane and tempera-

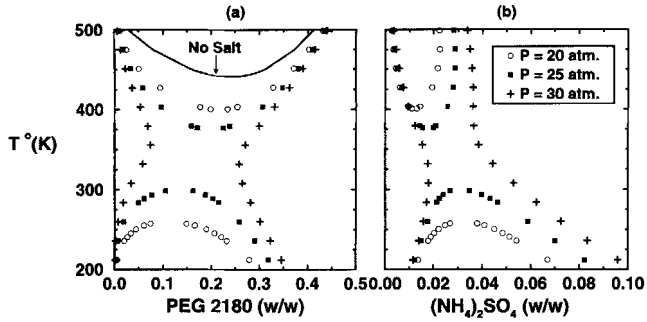

Figure 5. Theoretical phase diagrams in (a) temperature–PEG weight fraction plane, and (b) temperature–$(NH_4)_2SO_4$ weight fraction plane for a PEG 2180–$(NH_4)_2SO_4$–water mixture.

The solid line in (a) corresponds to the theoretical phase diagram of a PEG 2180–water mixture in the absence of salts.

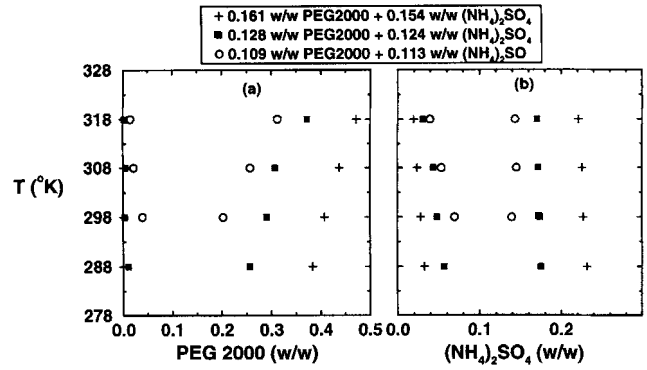

Figure 6. Experimental binodal data for a PEG 2000–$(NH_4)_2SO_4$ aqueous two-phase mixture from Voros et al. (1993).

Here, the binodal data have been plotted in the (a) T–PEG weight fraction plane, and the (b) T–$(NH_4)_2SO_4$ weight fraction plane. The binodal data have been obtained at four different temperatures for each of three mixtures containing different overall (before phase separation) concentrations of PEG and $(NH_4)_2SO_4$ as reported in the legend.

ture–$(NH_4)_2SO_4$ weight-fraction plane, respectively, at different osmotic pressures. The PEG-rich phases in Figure 5a (right branches of the phase diagram) correspond to the salt-deficient phases in Figure 5b (left branches of the phase diagram). In Figures 5a and 5b each symbol corresponds to an osmotic pressure at which the phase diagram of the mixture is calculated (see legend in Figure 5b). The solid line in Figure 5a corresponds to the phase diagram of the PEG 2180–water solution in the absence of the $(NH_4)_2SO_4$ salt.

Figures 5a and 5b show that at any fixed osmotic pressure, phase separation is seen in two regions, one corresponding to high temperature and the other corresponding to lower temperatures. The high-temperature phase separation is driven by the temperature-dependent Yukawa attraction between the PEG molecules (species 3) and is characterized by a LCST. The low-temperature phase separation, however, is driven by Coulombic interactions between salt ions (species 1 and 2) and is characterized by an upper critical solution temperature (UCST). Increasing the osmotic pressure lowers the LCST and increases the UCST until $P = 30$ atm, the phase diagrams merge. We believe that our model's predictions of both low-temperature and high-temperature phase separation could be related to the work of Weingärtner and coworkers (1991, 1992, 1995) and Narayanan and Pitzer (1994, 1995), who propose that in ionic solutions two types of phase separation can occur—one having to do with the long-ranged Coulombic interactions (Coulombic phase separation) and the other having to do with short-range attractions such as hydrogen bonding (solvophobic phase separation). Since the phase separation seen in PEG–salt–water aqueous two-phase systems is driven by the hydrogen bonding between the PEG and water and is solvophobic in nature, we focus here on the phase separation seen at high temperatures and compare these with the experimental PEG–salt–water phase diagrams.

In Figures 6a and 6b we present the experimental binodal data of Voros et al. (1993) for a PEG 2000–$(NH_4)_2SO_4$ aqueous two-phase system in the temperature–PEG weight fraction and temperature–$(NH_4)_2SO_4$ weight fraction planes, respectively. The binodal data were obtained at four different temperatures for each of three mixtures containing different overall (that is prior to phase separation) concentrations of PEG and $(NH_4)_2SO_4$, as reported in the legend.

It is not possible to make a direct comparison between our predicted phase diagrams (Figures 5a and 5b) and the experimental phase diagrams (Figures 6a and 6b) because we are unable to independently vary the equilibrium PEG and salt concentrations at a fixed temperature and pressure as is done in experiment. This is because we treat the PEG–salt–water solution as a pseudobinary mixture of PEG and salt which, according to the phase rule, means that there are only two degrees of freedom available to describe phase equilibrium. Thus fixing T and P automatically fixes the individual concentrations of the PEG and salt in each phase.

In our model PEG–salt–water mixture, at a fixed temperature, the equilibrium concentration of PEG and salt in each phase is varied by changing the osmotic pressure, P, of the mixture. In an experimental phase diagram (see Figures 6a and 6b), at a fixed temperature and pressure, the equilibrium concentration of PEG and salt in each phase is varied by changing the overall concentration of these components in the mixture prior to phase separation. Hence, varying the osmotic pressure in our model mixture is equivalent to varying the combined overall concentration of PEG and salt in the mixture (or the overall volume fraction, η) prior to phase separation. This approach of using the osmotic pressure as a variable to change the equilibrium concentration of a phase-separating mixture is not unusual and has been used by several investigators while modeling phase separation in polymer-colloid mixtures (Gast et al., 1983a,b), aqueous mixtures of polymer and protein (Vlachy et al., 1993; Mahadevan and Hall, 1990, 1992), micelle–water solutions (Reatto and Tau, 1984, 1985; Menon et al., 1991; Shukla and Rajagopalan, 1993), and micelle–salt–water mixtures (Kenkare et al., 1996).

We now compare the theoretical phase diagrams for our model PEG 2180–$(NH_4)_2SO_4$–water mixture (Figures 5a and 5b) with the experimental phase diagrams for a PEG 2000–$(NH_4)_2SO_4$–water mixture obtained from the binodal data of Voros et al. (1993) (Figures 6a and 6b). Figure 5a shows that an increase in the osmotic pressure lowers the

LCST for the mixture. For example, at osmotic pressures $P = 20$ and 25 atm the LCST is 400.8 K and 376.9 K, respectively. Our model also predicts that an increase in the osmotic pressure increases the miscibility gap by increasing the PEG concentration in the PEG-rich phases (right branch of phase diagram in Figure 5a) and the salt concentration in the salt-rich phases (right branch of phase diagram in Figure 5b). The experimental phase diagrams in Figures 6a and 6b show similar trends, that is, an increase in the overall concentration of each component in the mixture results in an increase in the miscibility gap and a decrease in the LCST of the mixture. The experimental phase diagrams, however, predict an LCST at temperatures below 300 K, whereas the theoretical phase diagrams predict that the lowest possible LCST is at ≈ 350 K. Also, the experimental phase diagrams show the average equilibrium weight fractions of $(NH_4)_2SO_4$ in the salt-rich and salt-poor phases (see Figure 5b) to be approximately 0.05 and 0.2, respectively, whereas the theoretical phase diagrams show the average equilibrium weight fractions of $(NH_4)_2SO_4$ in the salt-rich and salt-poor phases (see Figure 5a) to be approximately 0.01 and 0.03, respectively.

We believe that the model phase diagrams underestimate the equilibrium salt concentration and predict a higher LCST than the experimental phase diagrams because the model does not take into account the hydration of the salt ions and the short-ranged attraction between the salt ions and the PEG molecules. The hydrated water surrounding the salt ions could deplete the water that is bound to the PEG molecules (due to increased competition for water), thus increasing the attraction between the PEG molecules (due to reduced screening). This increase in attraction between the PEG molecules could then result in a further reduction in the LCST of the PEG–salt–water mixture. The short-ranged attractions between the salt ions and the PEG and the affinity of the cations to the ether oxygen in the PEG, both of which are neglected in our model but are present in a real system, could increase the equilibrium concentrations of salt in the PEG-rich and the PEG-poor phases in the PEG–salt–water mixture.

Our model (Figures 5a and 5b) predicts Coulombic phase instabilities at low temperatures that are not observed experimentally in PEG–salt–water mixtures. It is possible that this Coulombic phase separation actually exists but cannot be observed experimentally because it is preempted either by the crystallization of the PEG or salt or by the freezing of the water (Narayanan and Pitzer, 1994). However, it may also be possible that in aqueous systems the presence of water significantly screens the Coulombic forces and that phase separation is driven by solvophobic forces alone. If this is indeed the correct picture, our simple model (which assumes the water to be a structureless continuum) might be erroneously predicting a Coulombic phase separation at low temperatures by not accurately accounting for screening effects of water.

Evaluation of PEG–Salt Binodal Plots and Comparison with Experiments. In this section we obtain theoretical PEG–salt binodal plots for a variety of salts at a range of temperatures and PEG molecular weights and compare the trends seen with experiments. The PEG–salt binodal plots are obtained from osmotic pressure vs. concentration phase diagrams evaluated at constant temperature.

In Figures 7a and 7b, the theoretical PEG–$(NH_4)_2SO_4$–water phase diagrams are presented in the osmotic pressure vs. PEG weight-fraction and the osmotic pressure vs. salt weight-fraction planes, respectively, at a temperature $T = 350$ K. The osmotic pressure-concentration phase diagrams shown in Figures 7a and 7b are slices of the temperature-concentration phase diagrams shown in Figures 5a and 5b taken at $T = 350$ K. The horizontal lines are tie lines connecting pairs of equilibrium points (represented by filled circles) at the same osmotic pressures. The PEG-rich phase of the phase diagram in Figure 7a (the right branch) corresponds to the salt-poor phase of the phase diagram in Figure 7b (the left branch).

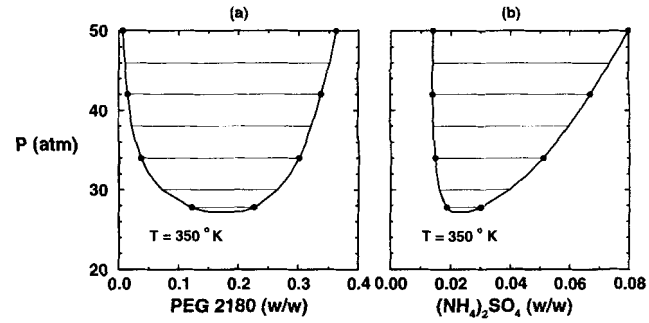

Figure 7. Theoretical phase diagrams in (a) osmotic pressure–PEG weight fraction plane, and (b) osmotic pressure–salt weight fraction plane at $T = 350$ K for the PEG 2180–$(NH_4)_2SO_4$–water mixture considered in Figures 5a and 5b.

The horizontal lines are tie lines connecting theoretical equilibrium points (filled circles) at the same osmotic pressure.

We generate PEG–salt binodal plots from osmotic pressure-concentration phase diagrams (such as those shown in Figures 7a and 7b) by plotting the PEG and salt weight fractions in each phase on a PEG weight-fraction vs. salt weight-fraction plot. Figure 8 presents the PEG 2180–$(NH_4)_2SO_4$ binodal curve at $T = 350$ K corresponding to the osmotic pressure-concentration phase diagrams in Figures 7a and 7b. The lines joining the points in the PEG-rich and salt-rich phases are tie lines that connect the equilibrium points at the same osmotic pressure and are identical to the tie lines shown in Figures 7a and 7b. In this discussion we only show theoretical binodal curves for the PEG–$(NH_4)_2SO_4$–water mixture at temperatures of 350 K and higher. Theoretical binodal curves evaluated at these temperatures correspond to phase separation in the LCST region and hence can be compared to experiments. At temperatures below 350 K, the two-phase regions begin at a UCST and thus cannot be compared with experiments.

Effect of Temperature on PEG – Salt Binodal Plots. We now study the effect of increasing temperature on the PEG 2180–$(NH_4)_2SO_4$ binodal curve. Figure 9a shows the theoretical PEG 2180–$(NH_4)_2SO_4$ binodal curves evaluated at temperatures $T = 350$ K and $T = 375$ K. In Figure 9b we plot the experimental PEG 2000–$(NH_4)_2SO_4$ binodal data obtained by Voros et al. (1993) at the temperatures $T = 288$ K and $T = 308$ K. The solid lines and dashed lines in Figures 9a and 9b are tie lines that represent the points in equilibrium at different temperatures. The theoretical binodal plots in Figure 9a show that an increase in the temperature increases

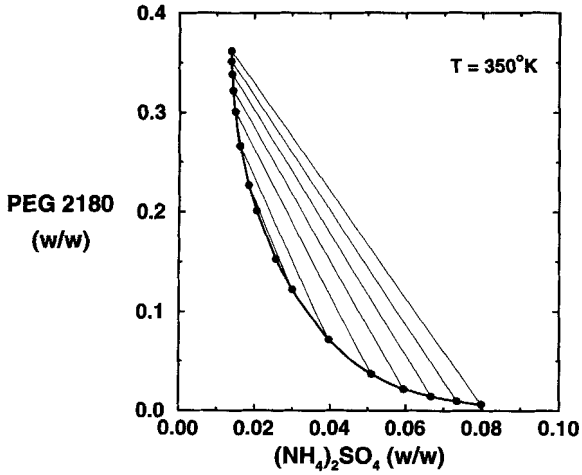

Figure 8. Theoretical PEG 2180–$(NH_4)_2SO_4$ binodal curve at 350 K obtained for the PEG 2180–$(NH_4)_2SO_4$–water system using the phase diagrams in Figures 7a and 7b.

The slanted lines are tie lines connecting the theoretical equilibrium points (filled circles) at the same osmotic pressure.

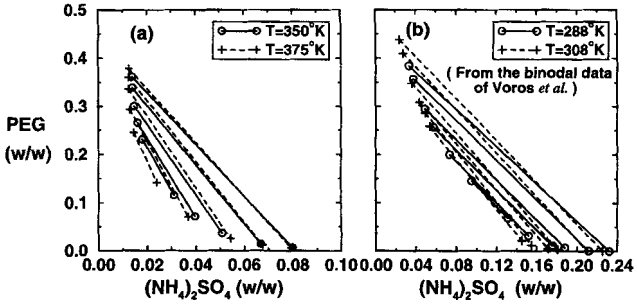

Figure 9. (a) Theoretical PEG 2180–$(NH_4)_2SO_4$ binodal curves evaluated at $T = 350$ K (○) and $T = 375$ K (+); (b) experimental binodal data from Voros et al. (1993) for the PEG 2000–$(NH_4)_2SO_4$–water mixture at $T = 288$ K and $T = 308$ K.

Solid and dashed lines for (a) are tie lines connecting points at equal osmotic pressure at $T = 350$ K and $T = 375$ K, respectively; for (b) are tie lines connecting the points in equilibrium at $T = 288$ K and $T = 308$ K, respectively.

the length and slope of the tie-lines—a trend that is also seen in the experimental data presented in Figure 9b. The theoretical temperature-concentration phase diagrams for this mixture (Figures 5a and 5b) show that at a fixed osmotic pressure an increase in temperature increases the concentration of PEG in the PEG-rich phase, but does not have much of an effect on the salt concentration in the salt-rich phase. This is why the tie lines on the binodal plot get longer and steeper with increasing temperature.

Effect of PEG Molecular Weight on PEG–Salt Binodal Plots. We now describe the effect of increasing the PEG molecular weight on the PEG–$(NH_4)_2SO_4$ binodal curve and compare the trends seen with experiments. Figure 10a presents the theoretical PEG–$(NH_4)_2SO_4$ binodal curves at $T = 350$ K for PEG of molecular weights 2,180, 5,000, and 8,000. Figure 10b presents the experimental PEG–$(NH_4)_2SO_4$ binodal data of Voros et al. (1993) at the temperature $T = 298$ K for PEG of molecular weights 1,000 and 2,000. The theory predicts that increasing the molecular weight moves the binodal curves toward lower PEG and lower salt concentrations, a trend that is consistent with experimental observation. The theoretical predictions, however, worsen with increasing PEG molecular weight. Figure 10a shows that the PEG-rich branches of the PEG 5000 and PEG 8000 binodal curves begin to curve back toward higher salt concentrations as the concentration of PEG increases—a result that is not observed experimentally.

We believe this discrepancy arises because the theory overestimates the excluded volume of the PEG molecules by modeling them as hard spheres. As the osmotic pressure of the mixture increases, the overall volume fraction of the PEG-rich phase increases, and this results in an increase in concentration of the hard-sphere PEG molecules in the PEG-rich phase. However, a further increase in osmotic pressure increases the overall volume fraction to an extent that even the smaller salt ions begin to enter the PEG-rich phase. This results in the binodal curves moving toward higher salt concentration. As the molecular weight of the PEG increases, this unphysical behavior begins to manifest itself at lower PEG concentrations. This is because at high PEG molecular weights the PEG-rich phase saturates at relatively low PEG concentrations because the size of the hard-sphere PEG molecules is quite large.

In reality the PEG molecules are interpenetrable. Hence even at higher overall volume fractions the PEG-rich phase does not get saturated because the PEG molecules can pack themselves effectively either through an overlap of the globular polymer coils for the low molecular weight PEGs, or through network formation for the high molecular weight PEGs.

Effect of Salt Type on PEG–Salt Binodal Plots. We now study the effect that different salts have on the theoretical PEG 2180–salt binodal curves. We consider three categories of salts: the first category contains salts with increasing anionic charge—NaOH, Na_2SO_4, and Na_3PO_4—the second category contains salts with increasing cationic charge—Na_2SO_4, $(NH_4)_2SO_4$ and $ZnSO_4$—and the third category

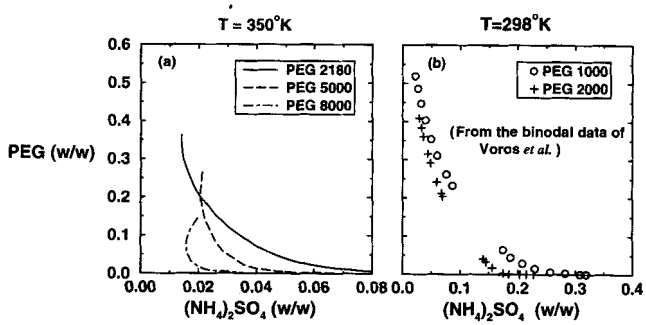

Figure 10. (a) Theoretical PEG–$(NH_4)_2SO_4$ binodal curves evaluated at $T = 350$ K for PEG of molecular weights 2,180, 5,000, and 8,000; (b) experimental PEG–$(NH_4)_2SO_4$ binodal data from Voros et al. (1993) at $T = 298$ K for PEG of molecular weights 1,000 and 2,000.

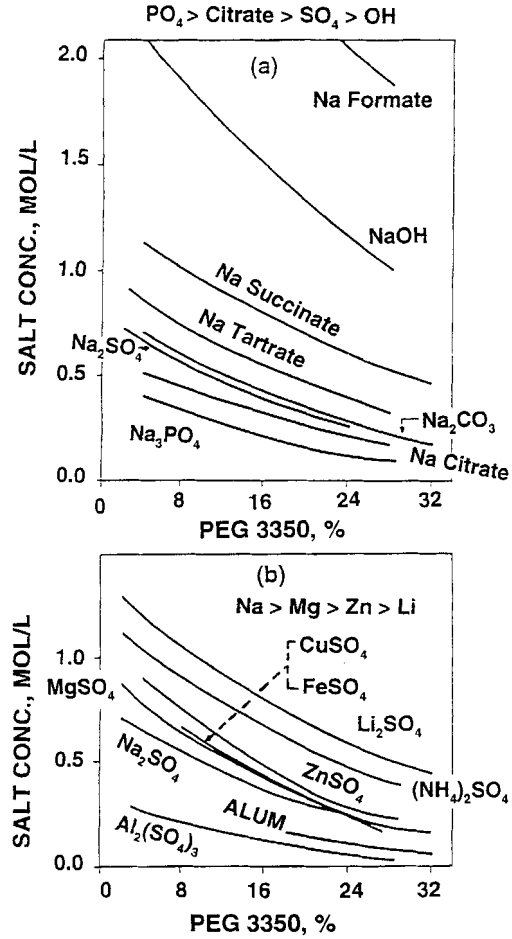

Figure 11. Experimental PEG 3350–salt binodal curves for inorganic salts from Ananthapadmanabhan and Goddard (1987).

(a) Binodal phase diagrams for PEG–Na salt aqueous two-phase systems; (b) binodal phase diagrams for PEG–metallic sulfate aqueous two-phase systems.

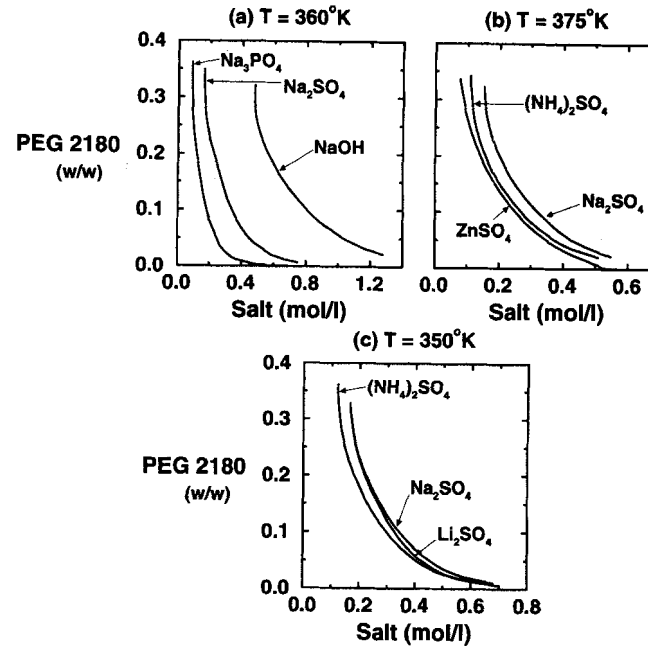

Figure 12. Theoretical PEG 2180–salt binodal curves: (a) at $T = 360$ K for the salts NaOH, Na_2SO_4, and Na_3PO_4 salts; (b) at $T = 375$ K for the salts Na_2SO_4, $(NH_4)_2SO_4$, and $ZnSO_4$; and (c) at $T = 350$ K for the salts $(NH_4)_2SO_4$, Na_2SO_4, and Li_2SO_4.

(a) The predicted movement of binodal curves toward lower salt concentrations with increasing cation charge is consistent with experimental observation. (b) The effect of increasing cation charge on the binodal curves is modeled. (c) The trends observed are inconsistent with experimental data. The model does a poor job of predicting the movement of the binodal curves with salts that have the same ratio of cation to anion charge (such as 1:2 above).

contains salts having the same anion (SO_4^{2-}) but different-sized monovalent cations—Li_2SO_4, Na_2SO_4, and $(NH_4)_2SO_4$. Theoretical binodal curves for the salts belonging to the first and second categories model the effect of increasing anion and cation charge, respectively, and the theoretical binodal curves for the third category model the effect of increasing ion size (keeping charge constant).

For each category of salts, the binodal curves are evaluated at a temperature that lies in the upper region of the "hour glass"-shaped temperature-concentration phase diagrams (see Figures 5a and 5b) for the PEG 2180–salt–water mixture. To facilitate the comparison between the trends predicted by our model and the measured PEG–salt binodal curves of Ananthapadmanabhan and Goddard (1987) (Figures 11a and 11b) we have expressed the binodal concentrations in units of PEG weight fraction and salt mol/L. Assuming that the density of the mixture equals 1 g/cm^3, the salt concentration in mol/L is calculated from the expression

$$\text{salt (mol/L)} \equiv (\text{salt w/w})(1{,}000)/(M_1 + M_2), \qquad (25)$$

where M_i is the atomic weight of ion i, and salt w/w is the salt weight fraction given by the expression in Eq. 21.

Figure 12a presents the theoretical PEG 2180–salt binodal curves for the salts NaOH, Na_2SO_4, and Na_3PO_4 (first category described earlier) at a temperature $T = 360$ K. The salts considered share a common cation (Na^+) but contain anions of increasing charge. The figure shows that increasing the charge on the anion from -1 (OH^-) to -3 (PO_4^{3-}) lowers the salt concentration at which phase separation occurs. Ananthapadmanabhan and Goddard (1987) observe an identical trend (see Figure 11a), that is, the effectiveness of the anion in forming an aqueous two-phase system with PEG is given by $PO_4^{3-} > SO_4^{2-} > OH^-$. Salts containing multivalent anions are better at forming an aqueous two-phase system with PEG than salts containing univalent anions because salts containing multivalent anions are better at lowering the LCST of a PEG–water solution (salting-out effect) than salts containing univalent anions. Ananthapadmanabhan and Goddard have postulated that anions with a higher valence are better salting-out agents than anions with a lower valence because the higher valence anion hydrates more water than the lower valence anion, thus decreasing the amount of water available to hydrate PEG. However, our model, which neglects hydration, predicts that the higher salting-out effective-

ness of the multivalent anions can be explained by charge effects alone. The inclusion of ion hydration into the theory could possibly improve the model's predictions by decreasing further the LCST of the phase-forming region from $T = 360$ K to room temperature.

Figure 12b presents PEG 2180–salt binodal curves for the salts Na_2SO_4, $(NH_4)_2SO_4$, and $ZnSO_4$ (second category) at a temperature $T = 375$ K. The salts considered have a common anion (SO_4^{2-}), but contain cations of increasing charge. The model predicts that increasing the charge on the cation lowers the salt concentration at which phase separation occurs. This is consistent with Ananthapadmanabhan and Goddard's (1987) result that $ZnSO_4$ is more effective than $(NH_4)_2SO_4$ in forming a two-phase system with PEG (see Figure 11b). However, our model incorrectly predicts that $ZnSO_4$ is more effective than Na_2SO_4 at forming an aqueous two-phase system with PEG. Ananthapadmanabhan and Goddard's (1987) results show that salts containing multivalent cations (e.g., Zn^{2+}) are not always better at forming a two-phase system with PEG than salts containing univalent cations (e.g., Na^+). Multivalent cations tend to form linkages with the ether oxygen of the PEG molecules (Ananthapadmanabhan and Goddard, 1987; Doscher et al., 1951; Schott, 1973; Schott et al., 1984), and the resulting complex that forms is thought to hydrate water. This water surrounding the PEG molecules screens the attraction between them and increases the LCST of the mixture (the "salting-in" effect). Hence, there are two competing effects in salts containing multivalent cations—the salting-out effect due to the higher charge on the cation (which our model can predict), and the salting-in effect due to the tendency of the cation to complex with the PEG (which our model cannot predict). For salts that complex with the PEG, an increase in salt concentration would increase complex formation and encourage hydration thus decreasing PEG–PEG attraction. Hence, for our model to predict the salting-in effect the PEG–PEG attraction would have to be made a function of salt type and salt concentration.

Figure 12c presents PEG 2180–salt binodal curves for the salts Li_2SO_4, Na_2SO_4 and $(NH_4)_2SO_4$ (third category) at the temperature $T = 350$ K. The salts considered have the same anion but different-sized cations of equal charge (+1). The model predicts that the phase-forming effectiveness of the salts is given by $(NH_4)_2SO_4 > Li_2SO_4 > Na_2SO_4$. The results, however, do not agree with the experimental binodal curves of Ananthapadmanabhan and Goddard (1987), who show that the phase-forming effectiveness of the salts is given by $Na_2SO_4 > (NH_4)_2SO_4 > Li_2SO_4$ (see Figure 11b). Because all three salts have the same ratio of anion-to-cation charge (1:2 in this case), charge effects are not responsible for the variations seen in the phase-forming effectiveness of the salts. Differences in solvent–salt interactions, such as hydration, and salt–PEG interactions, such as those caused by the complexation of the cations with the ether oxygen of the PEG, are probably factors that influence the variations seen in the phase-forming effectiveness of the salts. Our model ignores the just cited interactions and hence does a poor job of distinguishing between the phase-forming effectiveness of the salts.

A study of the trends exhibited by the theoretical binodal curves in Figures 12a and 12c indicate that by themselves excluded volume effects, resulting from a variation in anion or cation size ($SO_4^{2-} > PO_4^{3-}$ and $Na^+ > Li^+$), play a minor role in determining the phase-forming effectiveness of the salt. If excluded volume forces were important the theoretical binodal curves would predict the phase-forming effectiveness of the salts to be $Na_2SO_4 > Na_3PO_4$ in Figure 12a and $Na_2SO_4 > Li_2SO_4$ in Figure 12c. Charge effects and ion–solvent interactions play a more important role than excluded volume effects in determining the phase-forming effectiveness of the salt.

Conclusion

A simple model based in the integral-equation theory of statistical thermodynamics is used to study phase separation in a model PEG–salt–water mixture. The PEG molecules are modeled as hard spheres interacting via a temperature-dependent attractive Yukawa potential, the salt ions are modeled as charged hard spheres interacting via a Coulombic potential, and the water is a structureless continuum represented by a dielectric constant. The model ignores ion–solvent interactions (such as those due to hydration) and also assumes that the ion–PEG interactions are hard sphere alone. Thermodynamic properties for the mixture are evaluated using analytical solutions to the Ornstein–Zernike equation obtained by other investigators. Three adjustable parameters (z, A, and B) are used to fit the salt-free theoretical PEG–water phase diagram to the salt-free experimental PEG–water phase diagram. Once these three adjustable parameters are determined for each PEG molecular weight, no additional parameters are used to evaluate the phase diagrams for PEG–water mixtures in the presence of salts.

Theoretical phase diagrams in the temperature–PEG, temperature–salt weight-fraction planes, and PEG–salt weight-fraction planes (binodal curves) are obtained for a variety of salts and at a range of temperatures and PEG molecular weights. The model predicts several trends that are experimentally observed: (1) the presence of salt ions decreases the LCST of the PEG–water mixture; (2) an increase in temperature increases the miscibility gap of the PEG–salt–water mixture; (3) an increase in the PEG molecular weight moves the PEG–salt binodal curves toward lower PEG and salt concentrations; and (4) an increase in anion charge lowers the salt concentration at which phase separation occurs.

Our model also predicts Coulombic phase instabilities at low temperatures that are not observed experimentally in PEG–salt water systems. This could be either because the freezing of water preempts such a phase separation or because the presence of water significantly screens the Coulombic forces and that phase separation is driven by solvophobic forces alone. One way of confirming whether Coulombic interactions influence the phase behavior of PEG–salt mixtures at low temperatures is by determining phase diagrams of PEG–salt mixtures in solvents that freeze at temperatures lower than the freezing point of water and solvents that have a lower dielectric constant than water. In low dielectric constant solvents Coulombic interactions will dominate over solvophobic interactions, and in solvents that freeze at low temperatures phase diagrams can be determined at temperatures lower than that possible in water.

The theory has some shortcomings that nevertheless convey useful information concerning the relative importance of

ion–PEG interactions, ion–solvent interactions, and the interpenetrable nature of the PEG coils on the phase separation in PEG–salt aqueous two-phase systems. The theory underestimates the equilibrium salt concentration in the PEG-rich and salt-rich phases. This is probably because the theory ignores attractions between the PEG and salt ions originating either through dispersion forces or through the complexation of the salt cations with the ether oxygen in the PEG. The theory also predicts a higher LCST than is experimentally observed, most probably because hydration of the salt ions is ignored. Ion hydration probably depletes the water surrounding the PEG molecules (due to increased competition for water) and increases attraction between the PEG molecules (due to reduced screening), thus leading to a further decrease in the LCST of the mixture. We also observe that the theoretical predictions for the PEG–salt binodal curves worsen with increasing PEG molecular weight. We attribute this to our modeling of PEG molecules as hard spheres. PEG molecules in reality are interpenetrable; thus modeling them as hard spheres overestimates the volume occupied by them, especially in the PEG-rich phase, which in turn leads to incorrect binodal curves for high molecular weights of PEG.

Finally, a study of the trends exhibited by the theoretical binodal curves (Figures 12a–12c) indicate that charge effects and ion–solvent interactions play a more important role than excluded volume effects (resulting from a variation in anion or cation size) in determining the effectiveness of the salt in forming an aqueous two-phase system with PEG.

Acknowledgments

The authors gratefully acknowledge financial support from the National Science Foundation (Grants CTS-9208590 and CBT-8720284). In addition we would like to express our gratitude to Dr. Daniel Forciniti for many helpful discussions during the early stages of this work.

Literature Cited

Abbott, N. L., D. Blankschtein, and T. A. Hatton, "On Protein Partitioning in Two-Phase Aqueous Polymer Systems," *Bioseparations*, **1**, 191 (1990).

Abbott, N., D. Blankschtein, and T. A. Hatton, "Protein Partitioning in Two-Phase Aqueous Polymer Systems: 1. Novel Physical Pictures and a Scaling-Thermodynamic Formulation," *Macromol.*, **24**, 4334 (1991).

Abbott, N., D. Blankschtein, and T. A. Hatton, "Protein Partitioning in Two-Phase Aqueous Polymer Systems: 2. On the Free Energy of Mixing Globular Colloids and Flexible Polymers," *Macromol.*, **25**, 3917 (1992a).

Abbott, N., D. Blankschtein, and T. A. Hatton, "Protein Partitioning in Two-Phase Aqueous Polymer Systems: 3. A Neutron Scattering Investigation of the Polymer Solution Structure and Protein-Polymer Interactions," *Macromol.*, **25**, 3932 (1992b).

Abbott, N., D. Blankschtein, and T. A. Hatton, "Protein Partitioning in Two-Phase Aqueous Polymer Systems: 4. Proteins in Solutions of Entangled Polymers," *Macromol.*, **25**, 5192 (1992c).

Abbott, N., D. Blankschtein, and T. A. Hatton, "Protein Partitioning in Two-Phase Aqueous Polymer Systems: 5. Decoupling of the Effects of Protein Concentration, Salt Type, and Polymer Molecular Weight," *Macromol.*, **26**, 825 (1993).

Abrams, D. S., and J. M. Prausnitz, "Statistical Thermodynamics of Liquid Mixtures: A New Expression for the Excess Gibbs Energy of Partly or Completely Miscible Systems," *AIChE J.*, **21**, 116 (1975).

Albertsson, P.-Å., *Partition of Cell Particles and Macromolecules*, 3rd ed., Wiley-Interscience, New York (1986).

Ananthapadmanabhan, K., and E. Goddard, "Aqueous Biphase Formation in Polyethylene Oxide-Inorganic Salt Systems," *Langmuir*, **3**, 25 (1987).

Arrieta, E., C. Jedrzejek, and K. Marsh, "Numerical MSA Solution for Binary Yukawa Mixtures," *J. Chem. Phys.*, **86**, 3607 (1987).

Atha, D. H., and K. C. Ingham, "Mechanism of Precipitation of Proteins by Polyethylene Glycols," *J. Biol. Chem.*, **256**, 12108 (1981).

Baskir, J., T. A. Hatton, and U. W. Suter, "Thermodynamics of the Separation of Biomaterials in Two-Phase Aqueous Polymer Systems: Effect of the Phase-Forming Polymers," *Macromolecules*, **20**, 1300 (1987).

Baskir, J. N., T. A. Hatton, and U. W. Suter, "Protein Partitioning in Two-Phase Aqueous Polymer Systems," *Biotechnol. Bioeng.*, **34**, 541 (1989a).

Baskir, J., T. A. Hatton, and U. W. Suter, "Thermodynamics of the Partitioning of Biomaterials in Two-Phase Aqueous Polymer Systems: Comparison of Lattice Model to Experimental Data," *J. Phys. Chem.*, **93**, 2111 (1989b).

Blum, L., "Mean Spherical Model for Asymmetric Electrolytes I. Method of Solution," *Mol. Phys.*, **30**, 1529 (1975).

Blum, L., and J. Hoye, "Mean Spherical Model for Asymmetric Electrolytes. 2. Thermodynamic Properties and the Pair Correlation Function," *J. Phys. Chem.*, **81**, 1311 (1977).

Brooks, D., K. Sharp, and D. Fisher, "Theoretical Aspects of Partitioning," *Partitioning in Aqueous Two-Phase Systems*, H. Walter, D. E. Brooks, and D. Fisher, eds., Academic Press, Orlando, FL (1985).

Cabezas, H., Jr., J. D. Evans, and D. C. Szlag, "A Statistical Mechanical Model of Aqueous Two-Phase Systems," *Fluid Phase Equilib.*, **53**, 453 (1989).

Cabezas, H., Jr., J. D. Evans, and D. C. Szlag, "Statistical Thermodynamics of Aqueous Two-Phase Systems," *Downstream Processing and Bioseparation*, J.-F. P. Hamel, J. B. Hunter, and S. K. Sikdar, eds., American Chemical Society, Washington, DC (1990).

Diamond, A., and J. Hsu, "Fundamental Studies of Biomolecule Partitioning in Aqueous Two-Phase Systems," *Biotechnol. Bioeng.*, **34**, 1,000 (1989).

Diamond, A., and J. Hsu, "Protein Partitioning in PEG/Dextran Aqueous Two-Phase Systems," *AIChE J.*, **36**, 1017 (1990).

Döbert, F., A. Pfennig, and M. Stumpf, "Derivation of the Consistent Osmotic Virial Equation and Its Application to Aqueous Poly(ethylene glycol)-Dextran Two-Phase Systems," *Macromol.*, **28**, 7860 (1995).

Doscher, T., G. Myers, and D. Atkins, Jr., "The Behavior of Nonionic Surface Active Agents in Salt Solutions," *J. Colloid Sci.*, **6**, 223 (1951).

Edmond, E., and A. Ogston, "An Approach to the Study of Phase Separation in Ternary Aqueous Systems," *Biochem. J.*, **109**, 569 (1968).

Edmond, E., and A. Ogston, "Phase Separation in an Aqueous Quaternary System," *Biochem. J.*, **117**, 85 (1970).

Fisher, D., and I. A. Sutherland, eds., *Separations Using Aqueous Phase Systems*, Plenum Press, New York (1989).

Forciniti, D., and C. K. Hall, "Theoretical Treatment of Aqueous Two-Phase Extraction by Using Virial Expansions—A Preliminary Report," *Downstream Processing and Bioseparations*, J.-F. P. Hamel, J. B. Hunter, and S. K. Sikdar, eds., American Chemical Society, Washington, DC (1990).

Gast, A. P., C. K. Hall, and W. B. Russel, "Polymer-Induced Phase Separations in Nonaqueous Colloidal Suspensions," *J. Colloid Interf. Sci.*, **96**, 251 (1983a).

Gast, A. P., C. K. Hall, and W. B. Russel, "Phase Separations Induced in Aqueous Colloidal Suspensions by Dissolved Polymer," *Farad. Discuss. Chem. Soc.*, **76**, 189 (1983b).

Goldstein, R. E., "On the Theory of Lower Critical Solution Points in Hydrogen-bonded Mixtures," *J. Chem. Phys.*, **80**, 5340 (1984).

Guan, Y., T. H. Lilley, and T. E. Treffry, "Theory of Phase Equilibria for Multicomponent Aqueous Solutions: Applications to Aqueous Polymer Two-Phase Systems," *J. Chem. Soc. Farad. Trans.*, **89**, 4283 (1993a).

Guan, Y., T. H. Lilley, and T. E. Treffry, "A New Excluded Volume Theory and Its Application to the Coexistence Curves of Aqueous Polymer Two-Phase Systems," *Macromol.*, **26**, 3971 (1993b).

Guan, Y., T. H. Lilley, and T. E. Treffry, "Application of a Statisti-

cal Geometrical Theory to Aqueous Two-phase Systems," *J. Chromatog. A.*, **668**, 31 (1994).
Hansen, J.-P., and I. R. McDonald, *Theory of Simple Fluids*, 2nd ed., Academic Press, San Diego (1991).
Hartounian, H., E. Floeter, E. Kaler, and S. Sandler, "Effect of Temperature on the Phase Equilibrium of Aqueous Two-Phase Polymer Systems," *AIChE J.*, **39**, 1976 (1993).
Haynes, C., R. Beynon, R. King, H. Blanch, and J. Prausnitz, "Thermodynamic Properties of Aqueous Polymer Solutions: Poly(ethylene glycol)/Dextran," *J. Phys. Chem.*, **93**, 5612 (1989a).
Haynes, C., H. Blanch, and J. Prausnitz, "Separation of Protein Mixtures by Extraction: Thermodynamic Properties of Aqueous Two-Phase Polymer Systems Containing Salts and Proteins," *Fluid Phase Equilib.*, **53**, 463 (1989b).
Haynes, C., F. Benitez, H. Blanch, and J. Prausnitz, "Application of Integral-Equation Theory to Aqueous Two-Phase Partitioning Systems," *AIChE J.*, **39**, 1539 (1993).
Hill, T. L., *An Introduction to Statistical Thermodynamics*, Chap. 19, Addison-Wesley, Reading, MA (1960).
Kang, C., and S. Sandler, "Phase Behavior of Aqueous Two-Polymer Systems," *Fluid Phase Equilib.*, **38**, 245 (1987).
Kang, C., and S. Sandler, "A Thermodynamic Model for Two-Phase Aqueous Polymer Systems," *Biotechnol. Bioeng.*, **32**, 1158 (1988a).
Kang, C., and S. Sandler, "Effects of Polydispersivity on the Phase Behavior of Aqueous Two-Phase Polymer Systems," *Macromol.*, **21**, 3088 (1988b).
Karlström, G., "A New Model for Upper and Lower Critical Solution Temperatures in Poly(ethylene oxide) Solutions," *J. Phys. Chem.*, **89**, 4962 (1985).
Kenkare, P. U., C. K. Hall, and C. Caccamo, "Phase Instabilities in Charged Hard Sphere Mixtures. I. Binary Mixtures of Salt and Hard Spheres," *J. Chem. Phys.*, **103**, 8098 (1995a).
Kenkare, P. U., C. K. Hall, and C. Caccamo, "Phase Instabilities in Charged Hard Sphere Mixtures. II. Binary Mixtures of Salts," *J. Chem. Phys.*, **103**, 8111 (1995b).
Kenkare, P. U., C. K. Hall, and P. K. Kilpatrick, "The Effect of Salts on the Lower Consolute Boundary of a Non-Ionic Micellar Solution," *J. Colloid Interf. Sci.*, in press (1996).
King, R., H. Blanch, and J. Prausnitz, "Molecular Thermodynamics of Aqueous Two-Phase Systems for Bioseparations," *AIChE J.*, **34**, 1585 (1988).
Kjellander, R., and E. Florin, "Water Structure and Changes in Thermal Stability of the System Poly(ethylene oxide)-Water," *J. Chem. Soc., Farad. Trans.*, **1**, **77**, 2053 (1981).
Lee, L., *Molecular Thermodynamics of Nonideal Fluids*, Butterworths, London (1988).
Mahadevan, H., and C. K. Hall, "Statistical-Mechanical Model of Protein Precipitation by Nonionic Polymer," *AIChE J.*, **36**, 1517 (1990).
Mahadevan, H., and C. K. Hall, "Theory of Precipitation of Protein Mixtures by Nonionic Polymer," *AIChE J.*, **38**, 573 (1992).
Malcolm, G. N., and J. S. Rowlinson, "The Thermodynamic Properties of Aqueous Solutions of Polyethylene Glycol, Polypropylene Glycol and Dioxane," *Trans. Farad. Soc.*, **53**, 921 (1957).
Mansoori, G., N. Carnahan, K. Starling, and T. Leland, "Equilibrium Thermodynamic Properties of the Mixture of Hard Spheres," *J. Chem. Phys.*, **54**, 1523 (1971).
Menon, S., V. Kelkar, and C. Manohar, "Application of Baxter's Model to the Theory of Cloud Points of Nonionic Surfactant Solutions," *Phys. Rev. A*, **43**, 1130 (1991).
Monk, C. B., *Electrolytic Dissociation*, Chap. 14, Academic Press, New York (1961).
Narayanan, T., and K. S. Pitzer, "Critical Behavior of Ionic Fluids," *J. Phys. Chem.*, **98**, 9170 (1994).
Narayanan, T., and K. S. Pitzer, "Critical Phenomena in Ionic Fluids: A Systematic Investigation of the Crossover Behavior," *J. Chem. Phys.*, **102**, 8118 (1995).
Ogston, A., "Some Thermodynamic Relationships in Ternary Systems, with Special Reference to the Properties of Systems Containing Hyaluronic Acid and Protein," *Arch. Biochem. Biophys. Suppl.*, **1**, 39 (1962).
Reatto, L., and M. Tau, "A Statistical Model for Non-Ionic Micellar Solutions and Their Phase Diagrams," *Chem. Phys. Lett.*, **108**, 292 (1984).
Reatto, L., and M. Tau, "Statistical Model for Nonionic Micellar Solutions," *Physics of Amphiphiles: Micelles, Vesicles and Microemulsions*, V. Degiorgio and M. Corti, eds., North-Holland, Amsterdam, p. 448 (1985).
Seaki, S., N. Kuwahara, M. Nakata, and M. Kaneko, "Upper and Lower Critical Solution Temperatures in Poly(ethylene Glycol) Solutions," *Polymer*, **17**, 685 (1976).
Scheutjens, J., and G. Fleer, "Statistical Theory of the Adsorption of Interacting Chain Molecules: 1. Partition Function, Segment Density Distribution and Adsorption Isotherms," *J. Phys. Chem.*, **83**, 1619 (1979).
Scheutjens, J., and G. Fleer, "Statistical Theory of the Adsorption of Interacting Chain Molecules: 2. Train, Loop, and Tail Size Distribution," *J. Phys. Chem.*, **84**, 178 (1980).
Schott, H., "Salting In of Nonionic Surfactants by Complexation with Inorganic Salts," *J. Colloid Interf. Sci.*, **43**, 150 (1973).
Schott, H., A. Royce, and S. Han, "Effect of Inorganic Additives on Solutions of Nonionic Surfactants," *J. Colloid Interf. Sci.*, **98**, 196 (1984).
Shukla, K., and R. Rajagopalan, "Adhesive-hard-sphere Approximation for 'Vapor/Liquid' Transitions in Colloidal Dispersions," *Colloids Surf. A.*, **81**, 181 (1993).
Vlachy, V., H. Blanch, and J. Prausnitz, "Liquid-Liquid Phase Separation in Aqueous Solutions of Globular Proteins," *AIChE J.*, **39**, 215 (1993).
Voros, N., P. Proust, and A. Fredenslund, "Liquid-Liquid Phase Equilibria of Aqueous Two-Phase Systems Containing Salts and Polyethylene Glycol," *Fluid Phase Equilib.*, **90**, 333 (1993).
Walsh, G., and D. R. Headon, *Protein Biotechnology*, Chap. 3, Wiley, New York (1994).
Walter, H., D. E. Brooks, and D. Fisher, eds., *Partitioning in Aqueous Two-Phase Systems*, Academic Press, Orlando, FL (1985).
Walter, H., and G. Johansson, "Partitioning in Aqueous Two-Phase Systems: An Overview," *Anal. Biochem.*, **155**, 215 (1986).
Walter, H., G. Johansson, and D. E. Brooks, "Partitioning in Aqueous Two-phase Systems: Recent Results," *Anal. Biochem.*, **197**, 1 (1991).
Weingärtner, H., T. Merkel, U. Maurer, J. Conzen, H. Glasbrenner, and S. Käshammer, "On Coulombic and Solvophobic Liquid-Liquid Phase-Separation in Electrolyte Solutions," *Ber. Bunsenges. Phys. Chem.*, **95**, 1579 (1991).
Weingärtner, H., and E. Steinle, "p,T,x Surface of Liquid-Liquid Immiscibility in Aqueous Solutions of Tetraalkylammonium Salts," *J. Phys. Chem.*, **96**, 2407 (1992).
Weingärtner, H., M. Kleemeier, S. Wiegand, and W. Schröer, "Coulombic and Non-Coulombic Contributions to the Criticality of Ionic Fluids. An Experimental Approach," *J. Stat. Phys.*, **78**, 169 (1995).
Young, R. J., and P. A. Lovell, *Introduction to Polymers*, 2nd ed., Chapman & Hall, New York, p. 165 (1991).

Manuscript received Jan. 16, 1996, and revision received May 16, 1996.